Growth of sculpted forms in bedrock channels (Miño River, northwest Spain)

Miguel Ángel Álvarez-Vázquez[1,2,*] and Elena De Uña-Álvarez[1]

[1]Department of History, Art and Geography, University of Vigo (Spain), Ourense Campus, As Lagoas 32004-Ourense, Spain
[2]Instituto de Investigaciones Marinas (IIM-CSIC), Eduardo Cabello 6, 36208-Vigo, Spain

A total of 216 sculpted forms were registered on the granitic bedrock of the Miño River, northwest Iberian Peninsula. Analysis of *in situ* measurements (length, width and depth) revealed three general type-sets: incipient forms, longitudinal furrows and circular potholes. Maximum depth and upper radius (at the incision surface) were identified as key variables to mathematically determine the growth rate in each set. Three regression models are presented revealing that the development of the forms depends on a power law explaining their size and shape. Morphological and dimensional thresholds were established to better identify stages from incipient (active growth) and inherited (stationary growth) forms.

Keywords: Bedrock rivers, growth models, potholes, sculpted forms.

IN bedrock rivers, where the rock surface is exposed to the erosive action of water, a diversity of landforms is related to the fluvial incision. At the macroscale (kilometres), bedrock channels are affected by changes linked to the structure of the basin and oscillations of the base level[1–3]. At the meso- and microscale (metre–centimetre), the presence of joints and fractures in the rocks, and the turbulence of the flow determine the morphological patterns[4,5]. Fluvial landforms developed in the bedrock reflect the sensitivity of the system to change[6], presenting features resulting from several formative and degradative events[7,8]. The development of assemblages of minor erosive forms in the fluvial environment (potholes and other sculpted forms) usually lasts several thousands of years, even though there are evidences that fluvial potholes can be formed in about 60 years[9]. The analysis of these assemblages is a meaningful tool to understand the evolution of the fluvial system[10].

Descriptions of the morphology of sculpted forms differentiate three growth stages[11]: (i) an initial state of development represented by small cavities presenting flat or slightly concave bottoms; (ii) an intermediate stage, including deeper and often coalescent cavities with concave profile, and (iii) an advanced stage when the inner channels connect to single forms. The lowest points of the eroded rock are connected by runnels which diversify water flow among the bedrock ribs. The location and morphology of the fluvial sculpted forms play a crucial role in the control of water-erosive processes. Particularly, potholes (cavities with circular or semicircular opening) are an important part of the deepening process in bedrock channels[12,13].

In relation to potholes developed in Spanish bedrock rivers, Nemec *et al.*[14] and Lorenc *et al.*[15] described an evolutionary ranking based on the relationship between their dimensions and the cross-section morphology. According to Pelletier *et al.*[16], the hydraulic channel conditions and fluid mechanics can explain the growth of cylindrical potholes through time. Springer *et al.*[17,18] presented an empirical model and mentioned that mobile-erosion nodes (small cavities, furrows, flutes or scallops) may evolve to cylindrical cavities with stationary-erosion nodes (potholes). However, transition stages between both have not yet been clearly defined. Bigger potholes are generated near a knickpoint[19] and the presence of these forms can be significantly related to joints[20,21].

The present study addresses the growth of sculpted forms in a reach of the Miño River, northwest Spain. It takes into consideration the relevance of place-based knowledge in order to recognize the geodiversity related to the erosive action of water, and assess its dynamics at a reach scale. This acknowledgment is also highly significant for local management of fluvial spaces, since erosive forms are elements of the hydrological heritage.

Study area

The Miño River is the main water flow in the northwest of the Iberian Peninsula (Figure 1). In this sector, the organization of fluvial networks starts with the opening of the Atlantic Ocean (late Mesozoic), and its current configuration reflects the changes during the Palaeocene[22]. Rivers are deeply incised among flat areas as the result of glacio-eustatic changes (120 m base-level maximum oscillation) and uplift of the continental crust (rate 0.07–0.09 m ka^{-1})[23]. This explains a higher frequency of knickpoints towards the east, coinciding with fault lines.

The Miño runs along 317 km from its spring (Serra de Meira, 700 m amsl) to the Atlantic Ocean. In the upper
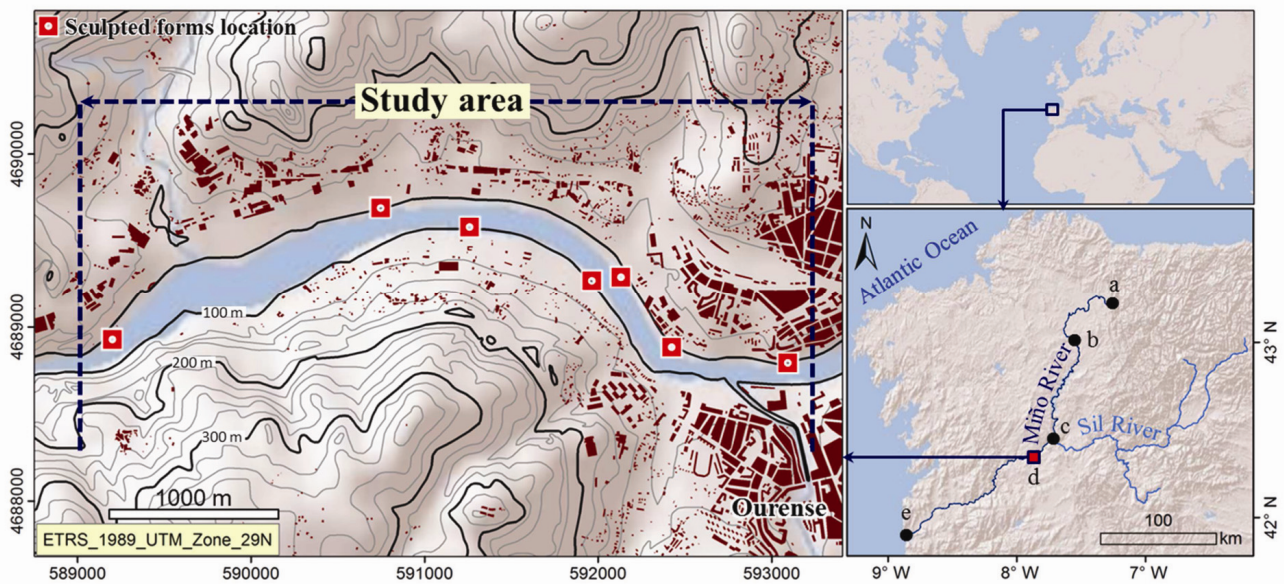
Figure 1. Map of the study area. Sites: (a) Serra de Meira, (b) Lugo, (c) Os Peares, (d) Ourense and (e) A Guarda. Basemaps ©2014 ESRI and ©IGN (MTN25).

Table 1. Factors of the Miño River, Ourense, Spain

Valley width (km)	3
Average height of channel (m)	100
Average gradient (slope, %)	0.07
Flow in natural regime ($m^3 s^{-1}$)	
Annual average	282.33
Minimum monthly (August)	77.80
Maximum monthly (December)	542.07
Minimum ecological flow ($m^3 s^{-1}$)	
October–December	55.414
January–Mars	74.449
April–June	54.004
July–September	38.445

Source: Ref. 24.

reaches the river flows over a flat area; downstream, after the town of Lugo, the river converges with the Sil River – its major tributary – in a stepped terrain (Os Peares). At the town of Ourense, the Miño goes through residual surfaces of 400 m amsl. The last 78 km of its course is the natural boundary between Spain and Portugal until its estuary (A Guarda). The river flow is regulated by several dams devoted mainly to hydropower.

The sampling area where minor erosive forms were recorded is a 6 km reach, in the mainstream of the Miño River running by Ourense. Riverbanks are heavily modified by human activity[24], presenting a significant flood risk. The lithology is composed by two-mica granite and granodiorite (Hercynian). Table 1 summarizes river features in the study area. The reach is located between two dams that regulate the flow and the base level; upstream is the Velle dam (27 m high, 17 cubic hectometer capa-

city) built in 1967, and downstream is the Castrelo dam (24 m high, 60 hm^3 capacity) operating since 1968; both are devoted to hydropower production. The area was also modified by the construction of bridges (the oldest was built in 1119 and rebuilt in 1672), roads and recreation walks. The average population density in the surrounding urban area is 1235 people km^{-2}. The presence of numerous hot springs and facilities for their exploitation is the main human activity.

Methods

The first sampling in 2011–12, linear in both riversides, generated an inventory that was revised and completed from 2013 to 2015, containing data from 216 sculpted forms. For each sample information relative to their dimensions was recorded, including (Figure 2): (i) maximum depth (D), or larger vertical axis from the bottom of the form to the surface of incision; (ii) horizontal length of the opening at the surface of incision level, largest diameter (S_{max}) and smallest diameter (S_{min}) and (iii) horizontal length of the bottom of the form, largest diameter (B_{max}) and smallest diameter (B_{min}).

An exploratory analysis was carried out to examine the dimensional relations between parameters, and appropriate statistical analysis was applied according to the distribution of the data. Three morphometric indexes were calculated: (i) a surface index (SI) defined as the relationship between the largest and smallest diameters at the surface of incision (SI = S_{max}/S_{min}); (ii) a bottom index (BI) being the relationship between diameters at the bottom of the form (BI = B_{max}/B_{min}); and (iii) a vertical index (VI) which expresses the relationship between the depth

Table 2. Summary statistics of the sculpted forms ($n = 216$)

Statistics	S_{max}	S_{min}	D	B_{max}	B_{min}
Minimum (cm)	10	5	2	7	4
Maximum (cm)	140	135	240	116	96
Range (cm)	130	130	238	109	92
Median (cm)	42	21	10	30	15
Average (cm)	45.12	26.41	20.08	36.43	19.74
Standard deviation	27.97	18.10	27.97	23.44	15.29
Standard error	1.90	1.23	1.90	1.59	1.04
Standardized skewness	5.87	13.81	21.18	5.86	13.07
Standardized kurtosis	3.16	25.63	57.39	1.13	17.15
Coefficient of variation (%)	54.97	68.53	139.29	64.34	77.48

Largest diameter at the surface (S_{max}), smallest diameter at the surface (S_{min}), maximum vertical depth (D), largest diameter at the bottom (B_{max}), smallest diameter at the bottom (B_{min}).
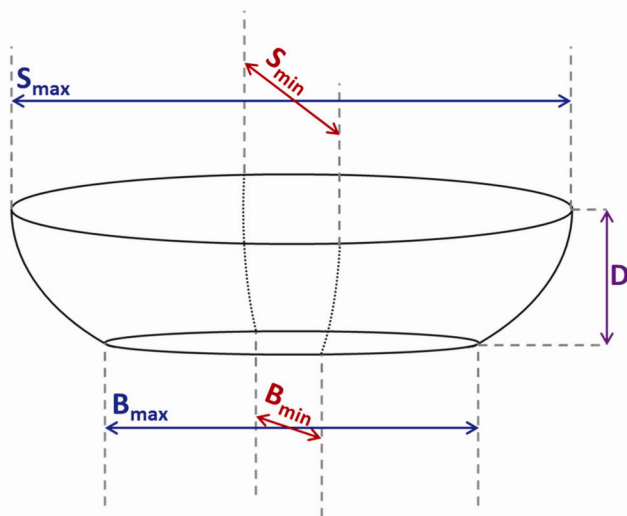

Figure 2. Fieldwork measures represented over an idealized sculpted form: S_{max} and S_{min} are the major and minor diameter at the upper horizontal opening respectively, B_{max} and B_{min} are the major and minor diameter at the horizontal bottom opening respectively. D is the maximum vertical depth.

of the erosive form and maximum radius ($r_{S_{max}} = S_{max}/2$) at the surface level (VI = $D/r_{S_{max}}$). Correlation and regression techniques were applied in order to find the growing patterns of erosive forms.

Results and discussion

The data collected for the 216 sculpted forms were statistically analysed (Table 2). Figure 3 presents the normality plots for the dimensional data. The standardized skewness and kurtosis were, in general, outside the range for a normal distribution (–2, +2), with medians being always under means. Rank correlations of Spearman, less sensitive to extreme values than the Pearson coefficients, showed statistically significant results (P-value <0.05, 95% confidence). A high direct correlation (0.92) was found between the largest diameter at the surface of incision (S_{max}) and the largest diameter at the bottom of the
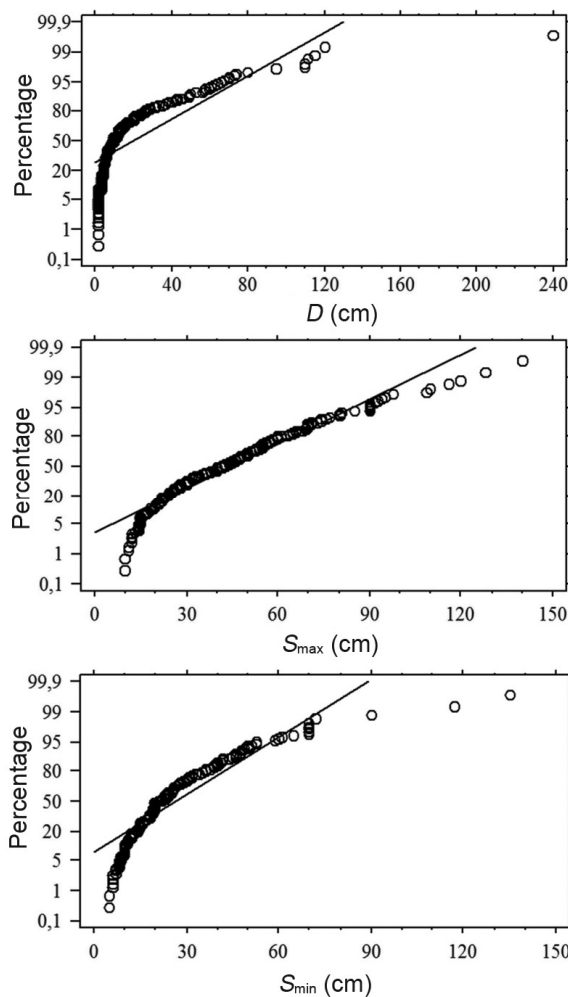
Figure 3. Normality plots for data distribution of depth (D), the maximum upper diameter (S_{max}) and the minimum upper diameter (S_{min}). The straight line is the adjustment by the least squares method to the theoretical normal distribution.

forms (B_{max}). The same was observed (0.89) for the smallest diameters (S_{min} and B_{min}) and so, only S_{max} and S_{min} were considered for further analysis. A statistically significant correlation was also found between the diameters at the surface (correlation between S_{max} and S_{min} was

0.76), and between depth (D) and the diameters at the surface of incision (D versus S_{max}, and D versus S_{min}, 0.78 and 0.85 respectively). Thus, the growth of the top and bottom horizontal apertures is linked to the deepening of erosive forms by a positive feedback.

Depending on the studied parameters (D, S_{max} and S_{min}), the 216 sculpted forms can be divided into three morphological sets (Figure 4).

(i) Set 1 ($n = 23$), namely incipient sculpted forms, including forms with a dimensional relation $S_{max} \approx S_{min} > D$, which are hemispherical ($n = 20$) or cylindrical ($n = 3$) forms, and have very low values for depth ($D < 20$ cm), length and width (S_{max} and $S_{min} < 60$ cm). Surface and bottom indexes are between 1.00 and 1.15 for the 75% of the forms (average SI = 1.08, and BI = 1.09). VI ranges from 0.27 to 0.83 (average 0.48).

(ii) Set 2 ($n = 134$) that includes groups with shallow, elongated, sculpted forms like furrows. Their general dimensional relation is $S_{max} > S_{min} > D$. They are hemiellipsoidal forms with concave profiles and low depth values ($D < 30$ cm), in which S_{max} is double the value of S_{min} in one half of the set. The average SI and BI are 2.19 and 2.38 respectively, and the highest values for these indexes in the inventory are found in this set (SI = 5.82 and BI = 6.67). The calculated values for VI range from 0.14 to 0.55.

Figure 4. Examples of sculpted forms for each set: (1) incipient forms, (2) elongated, furrow-like forms, and (3) potholes.

(iii) Set 3 ($n = 59$) includes potholes, with hemispherical ($n = 27$), hemihellipsoidal ($n = 3$) or cylindrical ($n = 29$) geometry, and complex profiles. Higher values of depth (D) mark the difference with the other two groups (Table 3), and the dimensional relation $S_{max} \approx S_{min} \geq D$ prevails. The surface and bottom indexes (SI and BI, average 1.18 and 1.11 respectively) are similar to set 1, the values calculated for the upper quantile (1.46 and 1.41 respectively) are indicative of oval openings. VI shows an average of 1.78 (range 0.70–3.69), indicating that these forms are deeper than the others under study.

According to the classification of Richardson and Carling[11], set 1 includes small cavities over horizontal surfaces that are sporadically flooded. Set 2 comprises mostly furrows with major axis that runs parallel or oblique to the main flow, their position and morphology are linked to the joint system. Set 3 comprehends the so-called potholes, mostly semi-submerged or submerged in the fluvial channel being strongly degraded. The relationship between the morphology of potholes and joints is clear by the presence of drop, kidney, multi-joint and lateral types as defined by Ortega et al.[21]. Some potholes presented a stepped cross-section, indicating several erosive sequences in their development. In general, as depth and diameter increase, sculpted forms evolve from simple into compound and coalescing morphologies (Figure 5 b). The thresholds for coalescence generation were 10 cm of depth (D) for cavities from set 1 (incipient forms), 50 cm of horizontal opening (S_{max}) for furrows (set 2), and potholes (set 3) coalesce when depth (D) and horizontal upper opening (S_{max}) reach 50 cm.

Set 1 and a large part of set 2 show similar features to those described for initial stages of potholes by Nemec et al.[14]. In these forms, the growth of the horizontal opening at the surface of incision prevails until the diameter equals the depth. After this threshold, potholes grow by lateral and vertical erosion[15]. This deepening (when $D > 40$ cm) clearly differentiates the development of potholes and furrows (Figure 5 a). The more developed furrows (set 2) contain circular cavities at their bottom with length and width over 15 cm, trapping sand and gravel, which could act as seeds of later potholes. Thus the transition from sets 1 and 2 to set 3 during the growing

Table 3. Summary statistics of D (maximum vertical depth in cm) by sets

| Statistics	Set 1	Set 2	Set 3
Count	23	134	59
Minimum	2	2	16
Maximum	17	28	240
Lower quartile	3	4	27
Median	5	6	45
Upper quartile	8	11	64
Outside points	Yes	Yes	Yes

process is possible. While potholes develop, there is a loss of symmetry in their morphology. Larger developed potholes have grooved walls, bottoms with central knolls and bulgy cross-sections; these features have been observed in the more developed forms of set 3.

Laboratory recreation of natural bedrock channels by Johnson and Whipple[7] indicates that robust erosive morphologies (potholes) can develop by feedbacks (between topography, erosion and sediment transport) only when slope in experimental design is higher than 10%; most of potholes in the studied reach, where the slope is ≈0.07%, may be inherited forms. According to the mechanistic model applied by Pelletier et al.[16], maximum bottom shear stress in the growth of the cylindrical potholes, if sediments are episodically emptied, is defined by D/mean radius = 1. It declines above this value, although the potholes continue growing until D/mean radius = 2; the development falls drastically thereafter. According to this, the values of vertical index (VI = $D/r_{S_{max}}$), presented in this work, may be interpreted as: (i) values of VI < 2 detect growing potholes, which increase their dimensions changing their morphology; (ii) values of VI > 2 are representative of slowly growing/stationary potholes, which also are the deepest recorded potholes ($n = 22$, depth between 56 and 240 cm); one pothole (VI = 3.69) is certainly an old inherited form.

In order to obtain the growth rate of potholes, Springer et al.[17] proposed the use of mean radius and depth. The forms where mean radius is greater than depth are mobile-erosion nodes that can create potholes; depth being

greater than the mean radius corresponds to stable-erosion nodes (potholes). As discussed earlier, D and S_{max} can differentiate between three sets of sculpted forms (Figure 5 a), and the vertical index (VI = D/r_{max}) indicates the potential of D and $r_{S_{max}}$ in the growth assessment of potholes. Note that in the sculpted forms with circular opening (sets 1 and 3), $r_{S_{max}}$ and the mean radius are similar, but mean radius does not provide enough information about the elongated forms included in set 2.

In Figure 6 a, the plot of $r_{S_{max}}$ versus D reveals two clear growth patterns. A regression analysis was performed considering D as the independent variable and $r_{S_{max}}$ as the dependent variable (outliers were not removed from the data). Table 4 presents the regression results by sets. The model presenting the lowest error of estimation was linear after data transformation into decimal logarithms (graphical representation in Figure 6 c); this result is coherent with that of Springer et al.[17], who reported that mean radius and depth in the potholes are related by
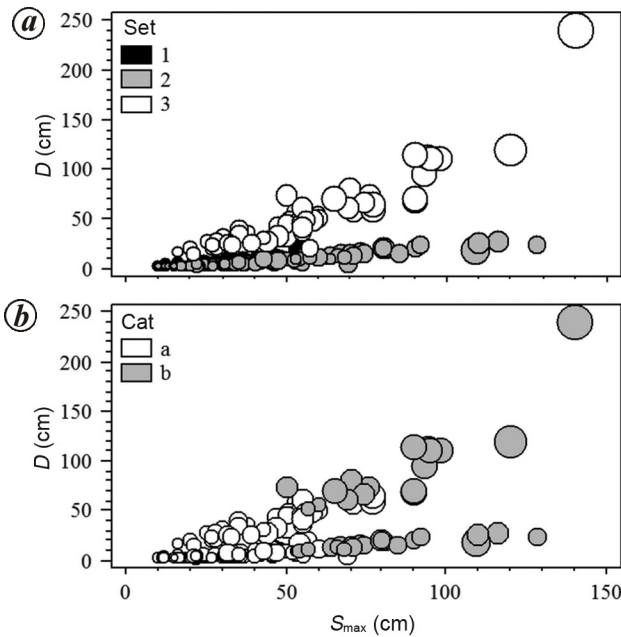
Figure 5. *a*, Vertical and horizontal growth by sets. *b*, Simple forms (cat a), and coalescent forms (cat b). D is the maximum depth and S_{max} is the major upper opening diameter. Bubble size is proportional to the minor upper opening diameter (S_{min}).
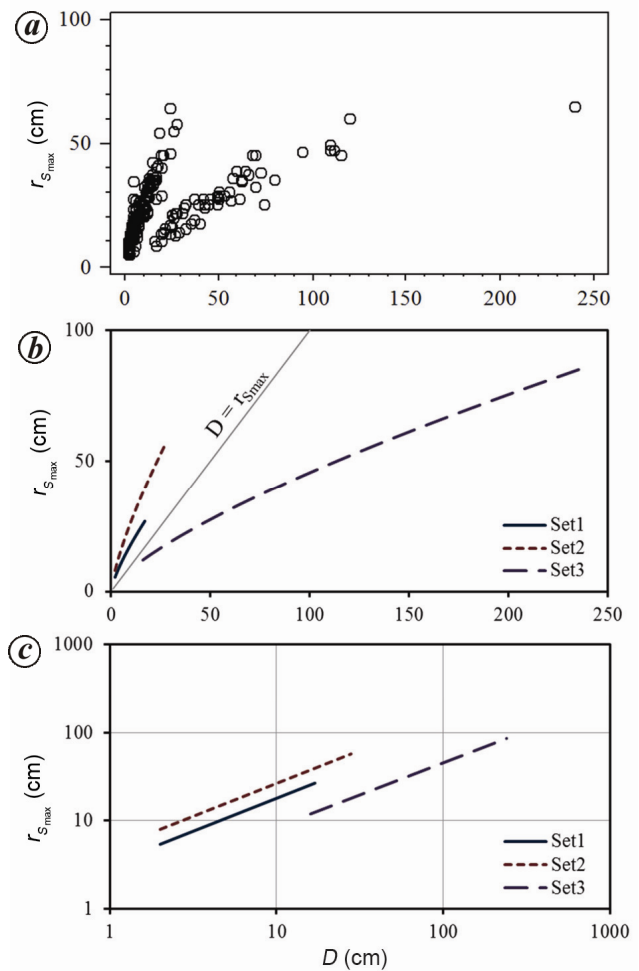
Figure 6. Plot of the major opening radius ($r_{S_{max}}$) versus maximum depth (D). *a*, Distribution of the samples. *b*, Regression models in a linear scale (grey line indicates the $D = r_{S_{max}}$). *c*, Regression models in a log–log scale.

Table 4. Regression models

Set	n	R^2	Equation	Power law	Error*
1	23	83.2	$\log(r_{S\max}) = 0.514 + 0.748 \cdot \log(D)$	$r_{S\max} = 3.27 \cdot D^{0.75}$	0.09
2	134	92.3	$\log(r_{S\max}) = 0.678 + 0.748 \cdot \log(D)$	$r_{S\max} = 4.76 \cdot D^{0.75}$	0.06
3	59	82.2	$\log(r_{S\max}) = 0.201 + 0.729 \cdot \log(D)$	$r_{S\max} = 1.59 \cdot D^{0.73}$	0.08

Confidence 99% (P-value < 0.01). *Standard error of estimate (slope).

a power law (linear correlation in log–log transformed data) along their growth. This log–log linear correlation is also applicable to elongated furrows and incipient forms, where the relationship $D = r_{S\max}$ (see Figure 6 b) clearly separates potholes ($D/r_{S\max} > 1$) and other morphologies ($D/r_{S\max} < 1$). The expression $\log(r_{S\max}) = a + b \cdot \log(D)$ can be reformulated, using antilogarithms, to the power law form $r_{S\max} = kD^b$ ($k = 10^a$), which is more suitable for comparison with the available literature.

The model equations explain the development of the studied sculpted forms, where opening (horizontal growth) and deepening (vertical growth) are related in different ways. The parameter b above indicates the proportionality of the increase of $r_{S\max}$ for any given value of depth (D). The results highlight a slightly higher proportional increase of the horizontal opening radius in the incipient forms and furrows of the sets 1 and 2 ($b = 0.75$), than in the potholes of set 3 ($b = 0.73$). These b coefficients are similar to, or in the range of, that obtained for potholes generated over other different lithologies[17,18,25]. The comparison with other kinds of sculpted forms was not possible because of lack of knowledge. Although the results for the b (<1) parameter suggest that deepening is faster than opening, in the range of D data of the studied sample (Table 3), this is true only for potholes with a depth higher than 20 cm; for incipient forms, furrows and shallow potholes the diameter grows faster than depth. The k coefficient, more meaningful in this case, indicates that horizontal opening growth follows the sequence set 2 > set 1 >> set 3. In order to properly assess the growth of sculpted forms, not only the b coefficient, but also the k parameter and total length of the opening (diameter) must be taken into account.

Conclusion

In the studied reach of the Miño River, the presence of currently growing and inherited sculpted forms, eroded in the granitic substrate, makes the area particularly suitable to examine the development of this kind of minor landforms. The analysis of the morphological and dimensional data allows differentiation of three main groups of forms (sets): the first group of shallow (incipient) forms, a second one containing elongated forms like furrows, and a third composed of potholes. Morphometric indexes were employed to identify the sculpted forms by their

stage of development. Regression models were developed for the three groups under study, well supported by statistical analysis of the correlation between depth and the longest radius at the horizontal upper opening. The results indicate that the horizontal growth (opening) is faster than the vertical incision (deepening), except for potholes with depth greater than 20 cm. Simple forms give way to coalescent configurations when depth reaches 10 cm (for incipient forms) or 50 cm (for potholes); the elongated furrows coalesce when the length of the horizontal opening diameter reaches 50 cm (like in potholes). The coalescing forms, presence of complex profiles and sculpted forms growing inside sculpted forms, support the view of different stages of development in the area. On comparison with other studies, the evolutionary pattern is found to be independent of lithology.

1. Tinkler, K. J. and Wohl, E. E., *Rivers over Rock: Fluvial Processes in Bedrock Channels*, America Geophysical Union, Monograph Series 107, Washington, 1998.
2. Wohl, E. E. and Merrit, D. M., Bedrock channel morphology. *Geol. Soc. Am. Bull.*, 2001, **113**(9), 1205–1212.
3. Ortega, J. A., Morfologías en los ríos en roca. In *Patrimonio geológico: los ríos en roca de la Península Ibérica* (eds Ortega, J. A. and Durán, J. J.), Publicaciones del Instituto Geológico y Minero de España, Madrid, 2010, vol. 4, pp. 55–77.
4. Whipple, K. X., Hancock, G. S. and Anderson, R. S., River incision into bedrock: mechanics and relative efficacy of plucking, abrasion, and cavitation. *Geol. Soc. Am. Bull.*, 2000, **112**(3), 490–503.
5. Hodge, R., Hoey, T. B. and Sklar, L. S., Bed load transport in bedrock rivers: the role of sediment cover in grain entrainement, translation, and deposition. *J. Geophys. Res.*, 2011, **116**; doi: 10.1029/2011JF002032.
6. Thomas, M. F., Landscape sensitivity in time and space, an introduction. *Catena*, 2001, **42**, 83–98.
7. Johnson, J. P. and Whipple, K. X., Feedbacks between erosion and sediment transport in experimental bedrock channels. *Earth Surf. Process. Landforms*, 2007, **32**(7), 1048–1062.
8. Turowski, J. M., Hovius, N., Hsieh, M. L., Lague, D. and Chen, M. C., Distribution of erosion across bedrock channels. *Earth Surf. Process. Landforms*, 2008, **34**, 26–37.
9. Kale, V. S. and Joshi, V. U., Evidence of formation of potholes in bedrock on human timescale: Indrayani river, Pune district, Maharashtra. *Curr. Sci.*, 2004, **86**(5), 723–726.
10. Brierley, G., Fryirs, K., Cullum, C., Tadaki, M., Huang, H. Q. and Blue, B., Reading the landscape: integrating the theory and practice of geomorphology to develop place-based understandings of river systems. *Prog. Phys. Geogr.*, 2013, **37**(5), 601–621.
11. Richardson, K. and Carling, P., A typology of sculpted forms in open bedrock channels. *Geol. Soc. Am., Spec. Pap.*, 2005, **392**, 1–108; http://specialpapers.gsapubs.org/content/392/1.full.pdf+html

12. Elston, E. D., Potholes: their variety, origin and significance. *Sci. Mon.*, 1917, **V**, 554–567.
13. Alexander, H. S., Pothole erosion. *J. Geol.*, 1932, **40**, 305–337.
14. Nemec, W., Lorenc, M. W. and Saavedra, J., Potholed granite terrace in the río Salor valley, western Spain: a study of bedrock erosion by floods. *Tecniterrae*, 1982, **50**, 6–21.
15. Lorenc, M. W., Muñoz, P. and Saavedra, J., The evolution of potholes in granite bedrock, W Spain. *Catena*, 1994, **22**, 265–274.
16. Pelletier, J. D., Sweeney, K. E., Roering, J. J. and Finnegan, N. J., Control on the geometry of potholes in bedrock channels. *Geophys. Res. Lett.*, 2015, **42**(3), 797–803.
17. Springer, G. S., Tooth, S. and Wohl, E. E., Dynamics of pothole growth as defined by field data and geometrical description. *J. Geophys. Res.*, 2005, **110**; doi: 10.1029/2005/F000321.
18. Springer, G. S., Tooth, S. and Wohl, E. E., Theoretical modelling of stream potholes based upon empirical observations from the Orange River, Republic of South Africa. *Geomorphology*, 2006, **82**, 160–176.
19. Sengupta, S. and Kale, V. S., Evaluation of the role of rock properties in the development of potholes: a case study of the Indrayani Knickpoint, Maharashtra. *J. Earth Syst. Sci.*, 2011, **120**(1), 157–165.
20. Wang, W., Liang, M. and Huang, S., Formation and development of stream potholes in a gorge in Guangdong. *J. Geogr. Sci.*, 2009, **19**(1), 118–128.
21. Ortega, J. A., Gómez-Heras, M., Pérez-López, R. and Wohl, E., Multiscale structural and lithologic controls in the development of stream potholes on granite bedrock rivers. *Geomorphology*, 2014, **204**, 588–598.
22. De Vicente, G. and Vegas, R., Large-scale distributed deformation controlled topography along the Western Africa–Eurasia limit: tectonic constraints. *Tectonophysics*, 2009, **474**, 124–143.
23. Viveen, W., Schoorl, J. M., Veldkamp, A., Van Balen, R. T., Desprat, S. and Vidal-Romaní, J. R., Reconstructing the interacting effects of base level, climate and tectonic uplift in the lower Miño terrace record: a gradient modelling evaluation. *Geomorphology*, 2013, **186**, 96–118.
24. Confederación Hidrográfica Miño-Sil, Plan Hidrológico 2015–2021: Parte española de la Demarcación Hidrográfica del Miño-Sil. MAGRAMA, Gobierno de España, 2014.
25. Kale, V. S. and Shingade, B. S., A morphological study of potholes of Indrayani Knick Point (Maharashtra). In *Exploration in Tropics* (eds Datye, V. S. *et al.*), Prof. K. R. Dikshit Felicitation Volume Committee, Pune, 1987, pp. 206–214.